Biointerface Research in Applied Chemistry
Open-Access Journal (ISSN: 2069-5837)

Article
Volume 16, Issue 1, 2026, 26
https://doi.org/10.33263/BRIAC161.026

Computational Evaluation of Sea Buckthorn Phytochemicals as CDPK3 and CDPK4 Inhibitors against *Plasmodium falciparum*

Wirdatun Nafisah [1,*], Gusnia Meilin Gholam [2], Riyan Alifbi Putera Irsal [3], Maheswari Alfira Dwicesaria [2], Elma Sakinatus Sajidah [1], Fatima Shahid [4,5], Fachrur Rizal Mahendra [2,6], David Herawan [7], Rahmah Muthmainnah Azam [8]

1 Biology Department, Faculty of Mathematics and Natural Science, Universitas Negeri Surabaya, Indonesia; wirdatunnafisah@unesa.ac.id (W.N.); elmasajidah@unesa.ac.id (E.S.S);
2 Department of Biochemistry, Faculty of Mathematics and Natural Sciences, IPB University, Bogor, Indonesia; gusniameilin@apps.ipb.ac.id (G.M.G); lec_mahesalfira@apps.ipb.ac.id (M.A.D); fachrurrizal@apps.ipb.ac.id (F.R.M);
3 Department of Applied Chemistry, Faculty of Engineering, Kyushu University, Japan; irsal.riyan.342@s.kyushu-u.ac.jp;
4 Department of Applied Physics, Faculty of Science and Technology, FST, University Kebangsaan Malaysia (UKM), Malaysia; fatima.shahid1492@yahoo.com;
5 Department of Industrial Biotechnology, Atta Ur Rahman School of Applied Biosciences, National University of Sciences & Technology, Islamabad, Pakistan;
6 Bioinformatics Research Center, Indonesian Institute of Bioinformatics (INBIO Indonesia), Malang, Indonesia
7 Department of Chemical Engineering, Faculty of Engineering, Universitas Indonesia, Jakarta, Indonesia; david.herawan@ui.ac.id;
8 Biotechnology Program, Graduate School, IPB University, Bogor, Indonesia; muthmainnahazam@apps.ipb.ac.id;
* Correspondence: wirdatunnafisah@unesa.ac.id;

Received: 6.08.2025; Accepted: 17.12.2025; Published: 15.02.2026

Abstract: Malaria remains a primary global health concern, and targeting proteins from the calcium-dependent protein kinase (CDPK) family of *Plasmodium falciparum* represents a novel and promising therapeutic strategy. In this study, we investigated the molecular interactions between sea buckthorn-derived compounds and *P. falciparum* CDPK3 and CDPK4 to address the unexplored antimalarial potential of this traditionally used medicinal plant. The active sites of each CDPK protein were predicted to facilitate docking analysis. *In silico* assessments of absorption, distribution, metabolism, and excretion (ADME), along with PASS, were used to evaluate drug-likeness properties and antiprotozoal potential. Density functional theory (DFT) calculations were performed to predict the electronic reactivity of potential inhibitors, and molecular dynamics (MD) simulations were used to evaluate complex stability. The results showed that the active sites of CDPK3 and CDPK4 were successfully identified, with 39 amino acid residues for CDPK3 and 105 for CDPK4. Molecular docking analyses demonstrated favorable binding affinities, ranging from 4.026 to 8.917 kcal/mol for the CDPK3–ligand complexes and from 5.072 to 11.09 kcal/mol for the CDPK4–ligand complexes. Among all evaluated compounds, oleanolic acid and ursolic acid exhibited the highest predicted drug-likeness and strong antiprotozoal activity, as supported by PASS predictions. DFT calculations further reinforced their inhibitory potential, with both compounds showing an extremely small energy gap difference of −0.0002 eV. In addition, MD simulations using normal mode analysis (NMA) showed that the candidate inhibitors formed stable complexes with both CDPK3 and CDPK4.

Keywords: *Hippophae rhamnoides*; HOMO-LUMO; normal mode analysis; quantum mechanics; *Plasmodium falciparum*; CDPK3; CDPK4.

1. Introduction

The most recent data on malaria cases, as reported in the 2025 publication, indicate that there are over 263 million cases and approximately 597,000 deaths annually. One of the critical contributing factors to this high disease burden is the widespread resistance of *Plasmodium falciparum* (*P. falciparum*) to nearly all frontline antimalarial drugs, posing a serious threat to current malaria control efforts [1]. The emergence of resistance to widely used antimalarial drugs, including artemisinin, has intensified the urgency to develop novel and effective therapeutic agents. In the drug discovery process, rational drug design has been recommended to target essential proteins or enzymes involved in the life cycle of malaria parasites. Consequently, a comprehensive understanding of the developmental stages of parasites has become critically important for the identification of new drug candidates. Calcium is known to act as a secondary messenger in signalling pathways that regulate the life cycle of *Plasmodium falciparum*. The calcium-dependent protein kinases (PfCDPKs) of *P. falciparum* are key mediators of calcium-triggered physiological processes in the parasite. The CDPK family in *P. falciparum* comprises one to seven members. Among these, CDPK3 and CDPK4 were identified as particularly significant. CDPK3 has emerged as a promising drug target owing to its expression during the ookinete stage, where it plays a crucial role in regulating ookinete motility, which is necessary for midgut invasion in mosquitoes. CDPK4 is involved in male gametocyte exflagellation and is essential for entry into the S-phase (DNA synthesis) in the rodent malaria parasite *P. berghei* [2–4]. Given the pivotal role of CDPKs in calcium signalling, targeting these kinases represents a promising strategy for both malaria treatment and prevention. However, despite their biological importance, CDPK3 and CDPK4 have rarely been simultaneously explored as dual molecular targets, leaving a substantial gap in the search for next-generation antimalarial drugs. Therefore, investigating these two kinases in parallel offers a novel perspective that integrates parasite developmental and transmission stages within a single therapeutic approach. This study addresses this critical challenge by exploring the therapeutic potential of sea buckthorn as a candidate antimalarial agent.

Sea buckthorn (*Hippophae rhamnoides* L.), a member of the Elaeagnaceae family, is a highly valued multipurpose shrub that predominantly grows in cold regions, such as the Indian Himalayas, China, Russia, and several countries in North America and Europe. In traditional medicine, the fruit of sea buckthorn has been widely utilized, particularly in Chinese herbal practices, owing to its broad-spectrum biological activities. It has gained significant attention for its applications in pharmaceuticals, cosmetics, bioenergy, and soil enrichment, largely attributed to its rich nutritional profile. Various studies have reported the presence of bioactive compounds with diverse therapeutic properties, including antitumor, antioxidant, hepatoprotective, and immunomodulatory effects. Recent findings also highlighted its potential as an anticancer agent (Figure 1) [5]. Nevertheless, its potential as an antimalarial agent, especially through the inhibition of calcium-dependent protein kinases, has not yet been reported. Thus, this study represents the first computational exploration of *H. rhamnoides*-derived compounds targeting CDPK3 and CDPK4 (CDPK3–4) in *P. falciparum*, providing new insights into an unstudied therapeutic avenue.

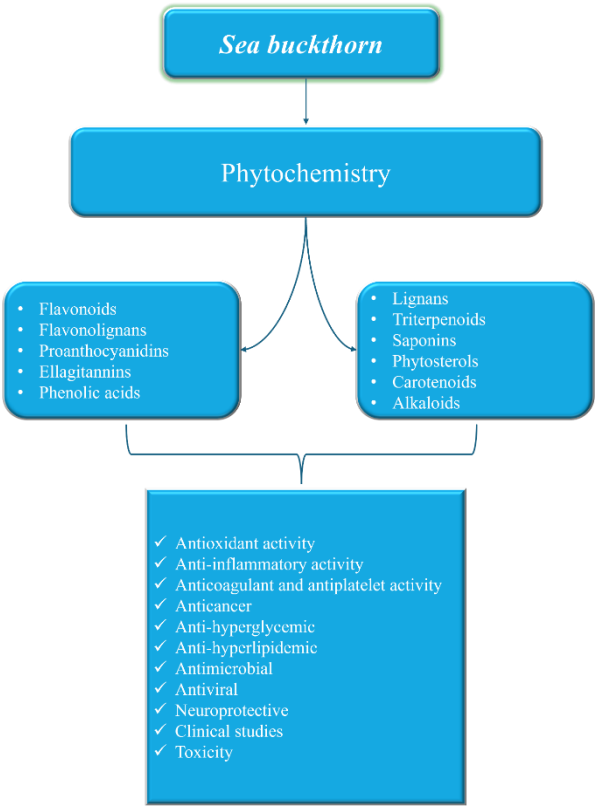

Figure 1. Pharmacological properties of sea buckthorn. Adapted from Zuchowski [6].

In the present study, we explored the mechanisms of action of a range of sea buckthorn-derived compounds that specifically target CDPK3 and CDPK4 (CDPK3-4). In this study, we aimed to identify potential inhibitors using an *in silico* computational approach. To ensure the reliability of the proposed candidates, the best-docked compounds were selected for further analysis based on their binding affinities, the stability of key hydrogen and hydrophobic interactions within the active site, and their relevance to previously reported pharmacological activities. These selection criteria were applied to prioritize ligands with strong molecular interactions and plausible drug-like characteristics for subsequent ADMET and pharmacokinetic evaluation. The research workflow is illustrated in Figure 2.

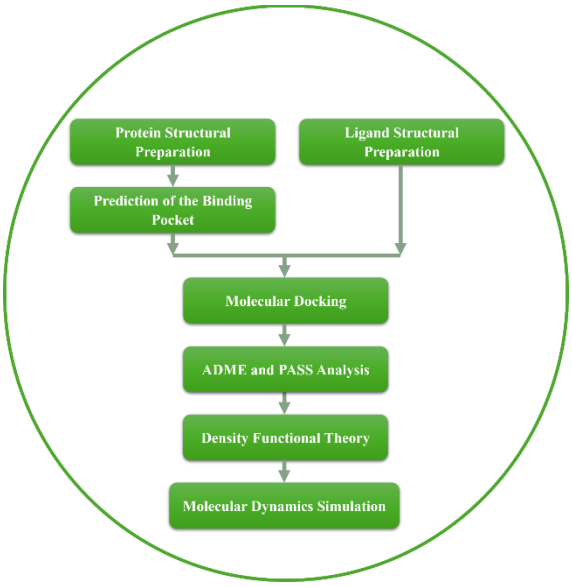

Figure 2. Research workflow to obtain inhibitor candidates for the CDPK3-4 protein in the search for new antimalarial drug candidates.

2. Materials and Methods

2.1. Protein preparation.

The three-dimensional structures of the target proteins *P. falciparum* CDPK3 and CDPK4 were retrieved from the RCSB Protein Data Bank via the respective links: CDPK3 (rcsb.org/structure/3K21) and CDPK4 (rcsb.org/structure/4RGJ) [7,8]. Protein structures were downloaded in PDB format and subsequently prepared for structural analysis. This preparation was performed using the YASARA Structure software and involved several steps, including the removal of water molecules, addition of hydrogen atoms, and application of quantum mechanics-based optimization using the PM3 method (QM-PM3). Prior to saving the structures in PDB format, energy minimization was performed on each target protein. This structural preparation was designed to ensure that the protein models were of high quality and suitable for reliable molecular docking simulations. The final prepared protein structures were then evaluated for quality using Ramplot (ramplot.in/) [9].

2.2. Ligand preparation.

The list of bioactive compounds from *Hippophae rhamnoides* used in this study as potential CDPK inhibitors was obtained from Pundir et al. [10]. All bioactive compounds, hereafter referred to as candidate inhibitors (ligands), were collected, and their 3D structures were retrieved from the PubChem database. Ligand preparation was performed using YASARA Structure to ensure proper preparation for molecular docking. The preparation steps included “clean all,” adjustment to the default physiological pH, and application of the NOVA optimization protocol. Several compounds previously reported and investigated as CDPK inhibitors were used as control inhibitors in this study. These control ligands served as a benchmark for evaluating key parameters, such as binding energy and the nature of amino acid residue contacts within the CDPK3-4 complex. Energy minimization was applied to all candidate and control ligands prior to docking simulations to enhance structural stability and accuracy of binding predictions [11].

2.3. Binding pocket prediction.

Binding pocket prediction of *P. falciparum* CDPK3 and CDPK4 target proteins was performed using CavityPlus (pkumdl.cn:8000/cavityplus#/). The prediction focused specifically on Chain A protein, with all advanced parameters maintained at their default settings. The protein structures uploaded for analysis were the pre-processed forms saved in PDB format, following prior structural preparation [12,13].

2.4. Molecular docking.

Specific molecular docking was conducted using YASARA Structure software. The VINA docking algorithm was employed, with the number of best poses per ligand set to “1” for output and reporting purposes. The docking results were primarily evaluated based on the binding energy values expressed in kcal/mol. During the simulation, the target proteins were treated as rigid structures, whereas the candidate inhibitors were modeled as flexible molecules. For the docking grid setup, the box dimensions for CDPK3 were configured as X = 68.89 Å, Y = 68.89 Å, and Z = 68.89 Å, whereas for CDPK4, the grid dimensions were set to X = 86.15 Å, Y = 86.15 Å, and Z = 86.15 Å. Both protein and ligand preparations were performed under

default pH conditions, which were consistently applied throughout the docking protocol. Additionally, the AMBER14 force field was employed to support docking energy calculations and enhance simulation accuracy [11].

2.5. ADMET and PASS prediction.

The selected candidate inhibitors were further evaluated for their pharmacokinetic profiles using the Absorption, Distribution, Metabolism, and Excretion (ADME) approach via the SwissADME platform (swissadme.ch/). For ligand preparation, the SMILES representations of each selected candidate inhibitor were retrieved individually from the PubChem database and used as inputs for ADME analysis. In parallel, docking validation was performed to assess the potential antiprotozoal activity of the compounds using the Prediction of Activity Spectra for Substances (PASS) online tool (way2drug.com/passonline/), with the same SMILES strings us for the prediction [14].

2.6. Density functional theory.

Theoretical molecular structures and geometric optimizations were performed using density functional theory (DFT) calculations with ORCA (ver. 5). Selected candidate inhibitors were first subjected to energy minimization using Avogadro software with the Universal Force Field (UFF). UFF was chosen because of its capability to accurately reproduce structural features and provide optimal geometries across diverse molecular systems. DFT calculations were performed using the def2-SVP basis set. The final output was generated with the "-molden" keyword to enable orbital visualization. The highest occupied molecular orbital (HOMO) and Lowest Unoccupied Molecular Orbital (LUMO) energy levels were subsequently visualized and analyzed using the IboView software. MEP calculation was performed using Avogadro.

2.7. Molecular dynamics simulation.

The dynamic behavior of the selected protein–ligand complexes was evaluated using the iMODS server. In advanced settings, the coarse-grained (CG) representation was set to "CA," deformation analysis was enabled ("Yes"), and the number of modes was specified as "20." The elastic network model was also considered during the simulation. The input for the analysis was the protein–ligand complex structure in ".pdb" format, which had been prepared and optimized in previous steps [15]. To obtain the root-mean-square fluctuation (RMSF), which calculates residue-level flexibility, this study employed CABS-flex (biocomp.chem.uw.edu.pl/CABSflex2/index).

3. Results and Discussion

3.1. Evaluation of protein preparation.

To ensure the structural quality of the prepared *P. falciparum* CDPK3-4 target proteins, validation analysis was conducted using the Ramachandran plot. As shown in Figure 3A, CDPK3 exhibited a high-quality structure, with 98.295% of residues in the favored regions, 1.705% in the allowed regions, and, notably, 0% in the disallowed regions. A similar quality profile was observed for CDPK4 (Figure 3B), which displayed 98.048% of the residues in the favored regions, 1.735% in the allowed regions, and only 0.217% in the disallowed regions.

These results indicate that the CDPK3 and CDPK4 structures were of acceptable quality for subsequent molecular docking studies.

Validation using the Ramachandran plot is widely recognized for identifying amino acid residues within the favored and disallowed regions of protein structures. Numerous studies have employed this method, such as the work of Kaur and Das [16], who modeled calcium-dependent protein kinase 2 (CDPK2) in potato (*Solanum tuberosum* L.) and validated the predicted 3D structure using a Ramachandran plot. This approach is well-established for assessing protein structure quality [17]. In malaria research, the 3D structure of *P. falciparum* calcium-dependent protein kinase 1 (PfCDPK1) was modeled using I-TASSER based on a FASTA-formatted amino acid sequence comprising 524 residues, and the model was subsequently validated using the Ramachandran plot [18]. Thus, based on the evaluation criteria presented, both receptors were deemed suitable for use in the docking simulations and for further investigation of their interactions with the selected molecules.

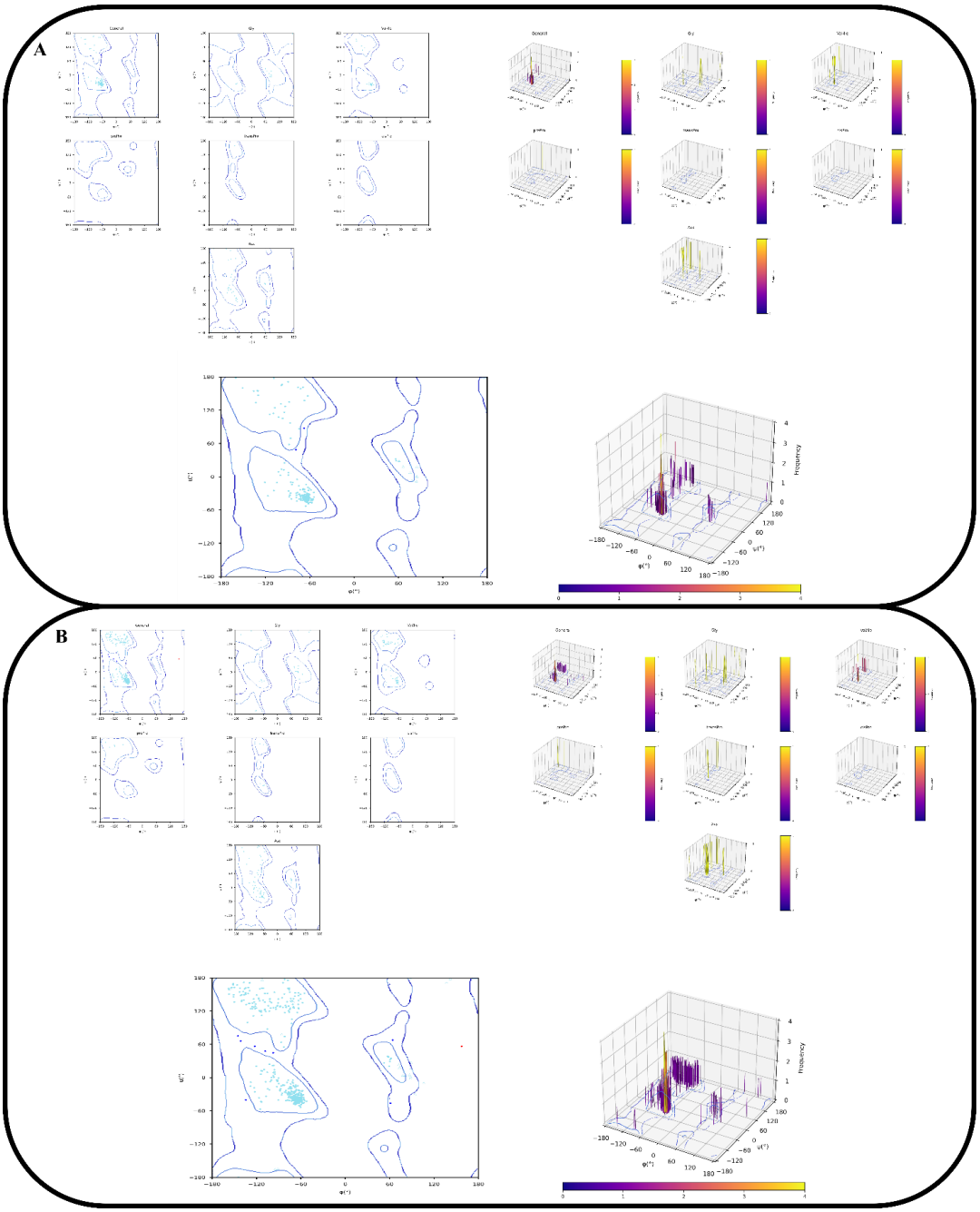

Figure 3. Evaluation of CDPK3-4 protein quality through Ramachandran plot post-protein preparation, (**A**) CDPK3 quality; (**B**) CDPK4 quality.

3.2. Binding pocket prediction.

To identify potential amino acid residues involved in ligand binding, we employed a binding-site detection method with CavityPlus. Choudhuri and Ghosh [19] explained that with the assistance of Cavity, it is possible to identify binding sites on the target receptor. Once these binding sites have been determined, deep learning can be applied to propose potential drug candidates based on predicted regions containing key residues.

Based on this analysis, the predicted binding pocket of CDPK3 consists of 39 amino acid residues, whereas that of CDPK4 comprises 105 residues (Figure 4). A complete list of the predicted amino acid residues with binding potential is presented in Table 1.

This study successfully predicted the key amino acid residues within the specific binding pockets of CDPK3 and CDPK4 that may interact with candidate inhibitors. This achievement was made possible by CavityPlus, which facilitated the identification of active-te residues crucial for *in silico* molecular docking studies [20]. Notably, the detected cavities or pockets within target proteins are predicted to play significant functional roles and are widely recognized as conventional ligand-binding sites. This approach has proven valuable for researchers in characterizing the binding pockets of target proteins whose allosteric potential has not been fully elucidated. The ability of ligands to bind to these predicted regions may further indicate the presence of allosteric mechanisms, thus supporting structure-based drug design strategies [21]. Thus, the residues identified will be used to assess whether the candidate molecules interact with the residues predicted by Cavity, which is expected to influence the biological function of the target receptors in *P. falciparum*.

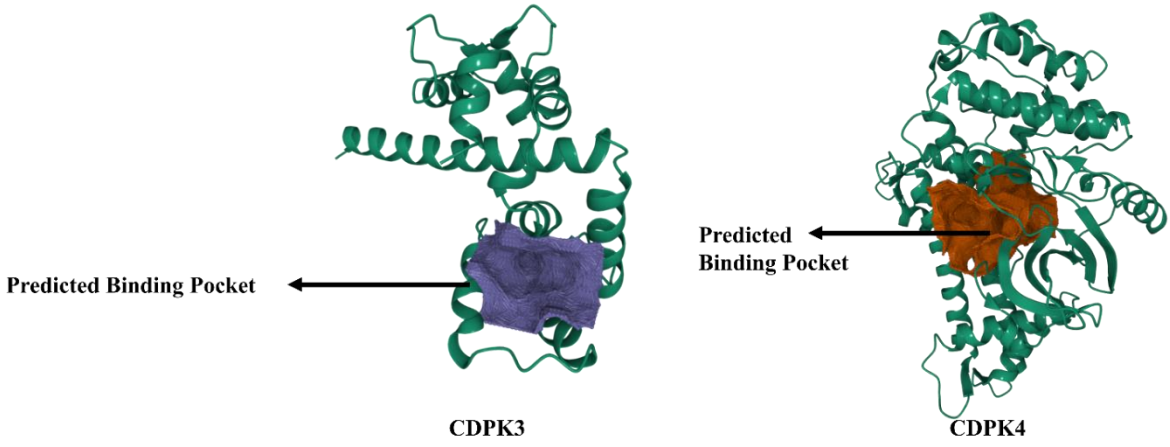

Figure 4. Binding pocket positions on the target proteins CDPK3 and CDPK4. Visualization generated using CavityPlus.

Table 1. Amino acid residues in the binding pocket of CDPK3-4.

Protein target	Surface area (Å^2)	Volume (Å^3)	Residues
CDPK3	398.25	696.25	VAL-60-A,LYS-84-A,LYS-53-A,THR-57-A,LEU-83-A,PRO-86-A,ALA-111-A,ASP-94-A,PHE-58-A,LEU-61-A,LEU-74-A,LEU-92-A,GLU-52-A,ILE-104-A,LEU-114-A,LEU-78-A,GLU-108-A,ASP-50-A,ASP-97-A,PHE-89-A,GLY-77-A,ARG-116-A,GLN-118-A,LEU-85-A,LYS-55-A,PHE-109-A,ALA-112-A,ALA-113-A,ASP-115-A,SER-98-A,SER-56-A,ILE-69-A,GLY-82-A,LEU-54-A,GLN-95-A,ASP-81-A,LEU-93-A,ILE-110-A,ILE-96-A
CDPK4	1712.50	2886.00	LYS-195-A,VAL-106-A,LEU-201-A,LEU-458-A,LYS-42-A,GLU-197-A,GLY-56-A,LEU-76-A,ALA-363-A,LYS-456-A,ASP-277-A,ALA-361-A,SER-460-A,SER-40-A,SER-491-A,THR-151-A,ILE-214-A,ALA-235-A,THR-461-A,ILE-75-A,LYS-231-A,LYS-466-A,LEU-464-A,GLY-82-

Protein target	Surface area (Å^2)	Volume (Å^3)	Residues
			A,ARG-455-A,GLU-83-A,ASP-157-A,GLU-158-A,SER-102-A,ALA-364-A,SER-161-A,ILE-43-A,GLU-223-A,LEU-200-A,LEU-53-A,PHE-471-A,TYR-367-A,SER-51-A,PHE-354-A,ILE-160-A,ILE-199-A,ASP-215-A,PHE-81-A,LEU-360-A,PHE-488-A,ILE-39-A,PRO-55-A,PRO-196-A,LYS-52-A,PHE-468-A,VAL-84-A,GLU-275-A,ARG-54-A,ASP-193-A,GLN-362-A,LYS-359-A,GLU-462-A,GLY-489-A,TYR-150-A,VAL-100-A,LEU-155-A,GLU-45-A,ILE-232-A,LYS-78-A,GLN-358-A,LEU-457-A,GLY-79-A,TYR-237-A,GLU-154-A,GLY-77-A,ASP-492-A,TYR-276-A,ASN-274-A,ARG-463-A,VAL-44-A,THR-357-A,SER-80-A,ALA-467-A,LEU-487-A,ILE-101-A,VAL-493-A,GLN-355-A,LYS-99-A,GLY-152-A,GLY-153-A,LEU-366-A,GLY-369-A,ILE-278-A,SER-370-A,GLY-272-A,LYS-469-A,ASN-198-A,LEU-365-A,LEU-470-A,THR-234-A,SER-273-A,GLY-233-A,PHE-156-A,LEU-459-A,SER-356-A,GLU-465-A,LEU-490-A,TYR-236-A

3.3. Post-docking analysis.

Molecular docking simulations were performed using the VINA algorithm and the AMBER14 force field, targeting the individual proteins CDPK3 and CDPK4. To the best of our knowledge, this study represents the first *in silico* investigation of compounds derived from sea buckthorn as novel antimalarial agents targeting two key proteins, CDPK3 and CDPK4 in *P. falciparum.*

This study employed molecular docking, which has been widely used in drug discovery and is considered effective for identifying potential antimalarial inhibitors. For instance, Lobato-Tapia *et al*. [22] employed docking to assess the interaction potential of compounds derived from *C. obtusifolia* with target proteins, using VINA-based binding energy calculations, a similar approach to that used in the present study. In malaria research, molecular docking has become a central computational technique in drug design, known for its significant contributions to hit identification and lead optimization [23].

Table 2 presents the top-ranked candidate ligands targeting CDPK3, ranked by binding energy. According to the results, casuarictin and casuarinin emerged as the top-performing ligands, with binding energy values of 8.917 and 8.795 kcal/mol, respectively. Notably, both ligands outperformed the three control ligands used in this study. Additionally, strictinin and oleanolic acid also showed promising binding energies, exceeding that of staurosporine, a well-established control ligand. Therefore, all candidate ligands exhibiting binding energy values higher than that of staurosporine were selected for further interaction analysis. The selected high-potential ligands included casuarictin, casuarinin, strictinin, and oleanolic acid. For comparative analysis of interactions with CDPK3, purfalcamine was also included as a reference ligand.

Table 2. Binding energy values in the CDPK3-ligand complex.

Rank	CID	Compound	Binding energy (kcal/mol)
1	73644	Casuarictin	8.917
2	442673	Casuarinin	8.795
3	24762166	Purfalcamine (Control inhibitor)	8.352
4	-	Compound 15 (Control inhibitor)	8.201
5	73330	Strictinin	7.818
6	10494	Oleanolic acid	7.779
7	44259	Staurosporine (Control inhibitor)	7.769
8	101051955	Dulcioic acid	7.557
9	64945	Ursolic acid	7.535
10	13917513	Isostrictinin	7.118
11	1794427	Chlorogenic acid	7.002
12	3081374	leucoanthocyanidins	7.002

Rank	CID	Compound	Binding energy (kcal/mol)
13	5281855	Ellagic acid	6.963
14	107876	Procyanidin	6.913
15	5281643	Quercetin-3-O-galactoside	6.906
16	5280863	Kaempferol	6.726
17	5280343	Quercetin	6.715
18	5281672	Myricetin	6.589
19	5281654	Isorhamnetin	6.5
20	72276	Epicatechin	6.49
21	72277	Epigallocatechin	6.443
22	10470	Octacosanoic acid	6.441
23	5280804	Quercetin-3–glucoside	6.352
24	65084	Gallocatechin	5.923
25	9064	Catechin	5.897
26	985	Palmitic acid	4.026

Figure 5 illustrates the two-dimensional interaction analysis of CDPK3-ligand complexes. The findings of this study reveal that casuarictin primarily engages in hydrogen bonding with CDPK3, without any observed hydrophobic interactions within the CDPK3–casuarictin complex (Figure 5A). A similar pattern was observed for casuarinin, which forms at least seven hydrogen bonds upon interaction with CDPK3 (Figure 5B). In the case of strictinin, hydrogen bonding also predominated; however, hydrophobic interactions were additionally established with the amino acid residues Ala111 and Ala112 (Figure 5C). In contrast to the aforementioned ligands, in which hydrogen bonding is the dominant interaction mode, oleanolic acid preferentially forms hydrophobic interactions with the CDPK3 protein (Figure 5D). A comparable interaction profile was observed for purfalcamine, the reference ligand, which also relies predominantly on hydrophobic interactions when binding to CDPK3 (Figure 5E). These results suggest that oleanolic acid shares similar binding characteristics with purfalcamine, highlighting the predominance of hydrophobic interactions in their respective complexes with CDPK3.

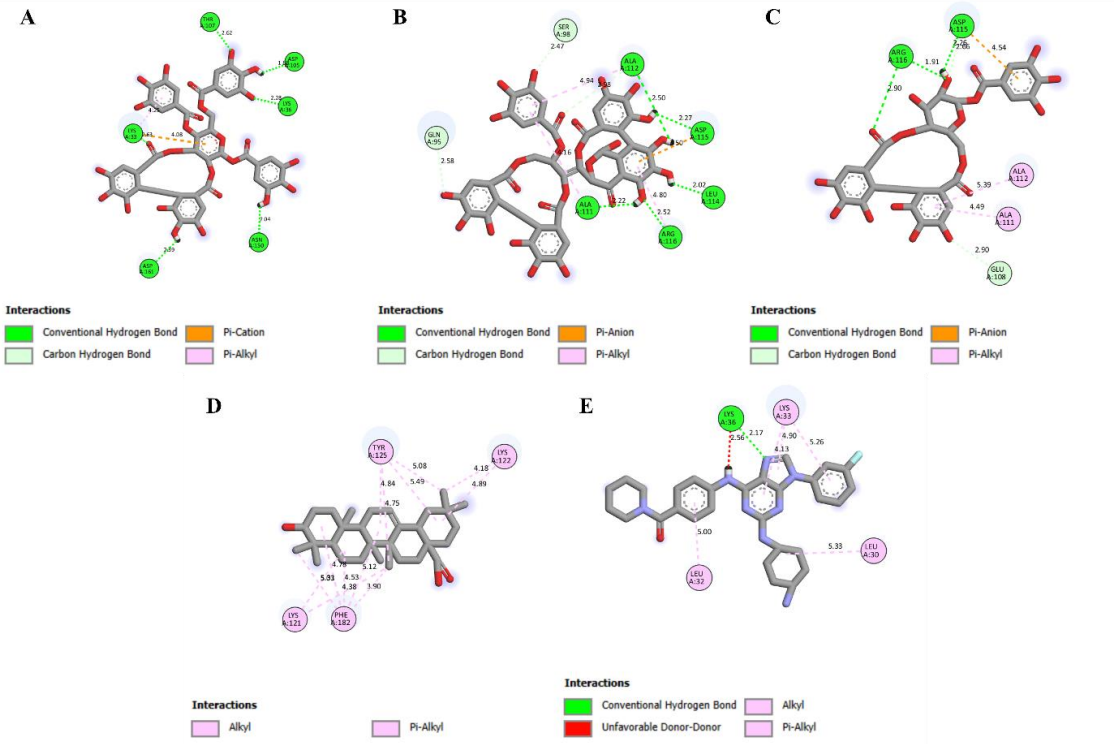

Figure 5. 2D interactions in the CDPK3-ligand complex, **(A)** Interaction of casuarictin with the CDPK3 target; **(B)** Interaction of casuarinin with the CDPK3 target; **(C)** Interaction of strictinin with the CDPK3 target; **(D)** Interaction of oleanolic acid with the CDPK3 target; **(E)** Interaction of purfalcamine (control ligand) with the CDPK3 target. 2D visualization was performed using BIOVIA Discovery Studio.

Table 3 presents the binding energy results, identifying casuarictin and ursolic acid as the top-ranked ligands. Both ligands exhibited higher binding affinity values than the three reference ligands, placing them at the top of the ranking. Consequently, casuarictin and ursolic acid were selected for further interaction analysis with CDPK4, whereas staurosporine was employed as the reference ligand for comparative interaction assessment with CDPK4.

Table 3. Binding energy values for the CDPK4-ligand complex.

Rank	CID	Compound	Binding energy (kcal/mol)
1	73644	Casuarictin	11.09
2	64945	Ursolic acid	11.068
3	44259	Staurosporine (Control inhibitor)	10.054
4	10494	Oleanolic acid	9.89
5	101051955	Dulcioic acid	9.775
6	-	Compound 15 (Control inhibitor)	9.664
7	107876	Procyanidin	8.766
8	73330	Strictinin	8.524
9	24762166	Purfalcamine (Control inhibitor)	8.472
10	442673	Casuarinin	8.449
11	5281672	Myricetin	8.407
12	5280863	Kaempferol	8.289
13	65084	Gallocatechin	8.282
14	5281855	Ellagic acid	8.261
15	13917513	Isostrictinin	8.2
16	5280343	Quercetin	8.153
17	5280804	Quercetin-3–glucoside	8.037
18	1794427	Chlorogenic acid	8.03
19	3081374	leucoanthocyanidins	8.03
20	5281643	Quercetin-3-O-galactoside	8.03
21	9064	Catechin	7.86
22	72277	Epigallocatechin	7.842
23	72276	Epicatechin	7.831
24	5281654	Isorhamnetin	7.469
25	10470	Octacosanoic acid	6.855
26	985	Palmitic acid	5.072

Casuarictin interacted with CDPK4 through both hydrogen bonding and hydrophobic interactions (Figure 6A). Notably, at least nine CDPK4 amino acid residues formed hydrogen bonds with casuarictin. These hydrogen bonds were observed to occur specifically with residues predicted as part of the binding pocket by CavityPlus. In contrast, ursolic acid engages in hydrophobic interactions with Lys359, a residue also identified by CavityPlus as a potential key binding site on CDPK4 (Figure 6B). Similarly, the reference ligand staurosporine formed both hydrogen bonds and hydrophobic contacts with the predicted pocket residues, further confirming the validity of the CavityPlus predictions (Figure 6C).

In this study, the evaluation of ligand–receptor interaction strength was not limited to the binding energy values expressed in kcal/mol. Instead, the identification and characterization of ligand interactions with specific amino acid residues were examined. This approach is essential because analyzing interactions within a receptor–ligand complex is a key step in understanding its binding properties. These binding properties may include electrostatic forces, hydrophobic interactions, and hydrogen bonding, all of which can contribute to enhancing binding affinity [24].

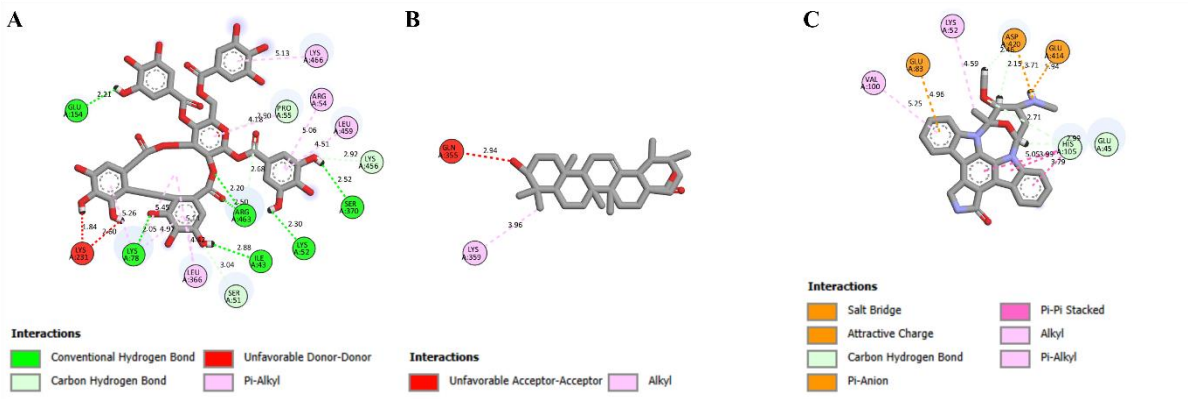

Figure 6. 2D interactions in the CDPK4-ligand complex, **(A)** Interaction of casuarictin with the CDPK4 target; **(B)** Interaction of ursolic acid with the CDPK4 target; **(C)** Interaction of staurosporine (control ligand) with the CDPK4 target. 2D visualization was performed using BIOVIA Discovery Studio.

3.4. ADME and PASS analysis.

To obtain the ADME profiles of the candidate compounds, we performed *in silico* predictions using SwissADME, while their individual antiprotozoal properties were evaluated using the PASS server (Way2Drug). Based on the ADME predictions, at least four candidates were identified as having limitations in drug-likeness according to Lipinski's Rule of Five. Casuarictin was classified as non-drug-like due to three rule violations, a characteristic also observed in strictinin, procyanidin, and casuarinin. In contrast, oleanolic acid, ursolic acid, and dulcioic acid exhibited favorable drug-likeness profiles, fulfilling Lipinski's criteria and thereby showing promise for oral drug development (Table 4). Furthermore, antiprotozoal activity predictions revealed that oleanolic acid, ursolic acid, and dulcioic acid displayed higher Pa values than Pi, suggesting their strong potential as antiprotozoal agents (Table 4). We employed the PASS server in this study, given its utility for identifying bioactive properties of compounds, especially in the historically underexplored field of antiprotozoal drug discovery, a field that has received significantly less attention than the development of antibacterial or antiviral agents. The persistent reliance on legacy therapeutics has led to a decline in efficacy, particularly in *Plasmodium* infections, where drug resistance has been increasingly reported. For instance, the spread of artemisinin-resistant *P. falciparum* in Southeast Asia and the declining effectiveness of pentavalent antimony compounds against visceral leishmaniasis in India underscore the urgent need for novel therapeutic options [25]. Additionally, ADME profiling plays a crucial role in predicting pharmacokinetic behavior and safety profiles of each candidate compound [14,26]. Therefore, identifying next-generation antiprotozoal agents is essential to developing more effective and safer therapeutic alternatives.

Table 4. ADME profile and antiprotozoal prediction of candidate inhibitors.

Compound	CID	Lipinski	Bioavailability Score	Synthetic accessibility	PASS value (Antiprotozoal) - Pa	PASS value (Antiprotozoal) - Pi
Casuarictin	73644	No; 3 violations: MW>500, NorO>10, NHorOH>5	0.17	7.35	0.209	0.050
Oleanolic acid	10494	Yes; 1 violation: MLOGP>4.15	0.85	6.08	0.246	0.073
Dulcioic acid	101051955	Yes; 1 violation: MLOGP>4.1	0.85	6.12	0.165	0.097
Strictinin	73330	No; 3 violations: MW>500,	0.17	5.94	0.233	0.033

Compound	CID	Lipinski	Bioavailability Score	Synthetic accessibility	PASS value (Antiprotozoal) - Pa	PASS value (Antiprotozoal) - Pi
		NorO>10, NHorOH>5				
Ursolic acid	64945	Yes; 1 violation: MLOGP>4.15	0.85	6.21	0.258	0.066
Casuarinin	442673	No; 3 violations: MW>500, NorO>10, NHorOH>5	0.17	7.93	0.176	0.083
Procyanidin	107876	No; 3 violations: MW>500, NorO>10, NHorOH>5	0.17	5.64	0.454	0.013

3.5. Density functional theory calculations.

This study employed density functional theory (DFT) calculations to evaluate the HOMO and LUMO energy levels of selected compounds using the ORCA quantum chemistry package. All calculations were conducted using the def2-SVP basis set. Based on the computed electron density distributions, oleanolic acid exhibited a HOMO energy level of –0.2142 eV and a LUMO of –0.0466 eV, while ursolic acid showed a HOMO of –0.2155 eV and a LUMO of –0.0466 eV (Figure 7). The inclusion of HOMO–LUMO analysis in this study is critical, as both are widely recognized as fundamental parameters in quantum chemistry [27]. The Highest Occupied Molecular Orbital (HOMO) refers to the highest energy level of a molecule that is still occupied by electrons and reflects its ability to donate electrons. Conversely, the Lowest Unoccupied Molecular Orbital (LUMO) represents the lowest available energy state that is not yet occupied, indicating the molecule's potential to accept electrons. Together, the HOMO and LUMO values define the energy gap, a parameter that plays a pivotal role in determining a molecule's chemical reactivity and biological activity[28]. In this study, the energy gap between HOMO and LUMO for oleanolic acid and ursolic acid was found to be remarkably similar, with a difference of only –0.0002 eV—calculated as –0.1687 eV and –0.1689 eV, respectively (Figure 7). This narrow gap suggests that both compounds possess comparable electronic reactivity, further supporting their potential as bioactive ligands targeting CDPK3-4.

A study by Abisek *et al*. [29], which investigated Barleria buxifolia root compounds targeting malarial PI4KIIIβ, reported the use of DFT calculations. In their study, the highest-energy outer orbital electrons were predicted to act as electron donors, known as the HOMO. In contrast, the lowest-energy inner orbital, referred to as the LUMO, functions as the electron acceptor and possesses sufficient space to receive electrons. The HOMO and LUMO orbitals help regulate the interactions between one molecule and another. Moreover, these orbitals may also assist in estimating kinetic stability and chemical reactivity within the band space. In another study on antimalarial compound discovery, Alruwaili et al. [30] employed DFT calculations based on quantum-mechanical (QM) techniques to estimate the electronic structure of molecules, atoms, and compounds. Therefore, the application of DFT calculations is highly relevant in antimalarial drug discovery and remains applicable to the context of the present study.

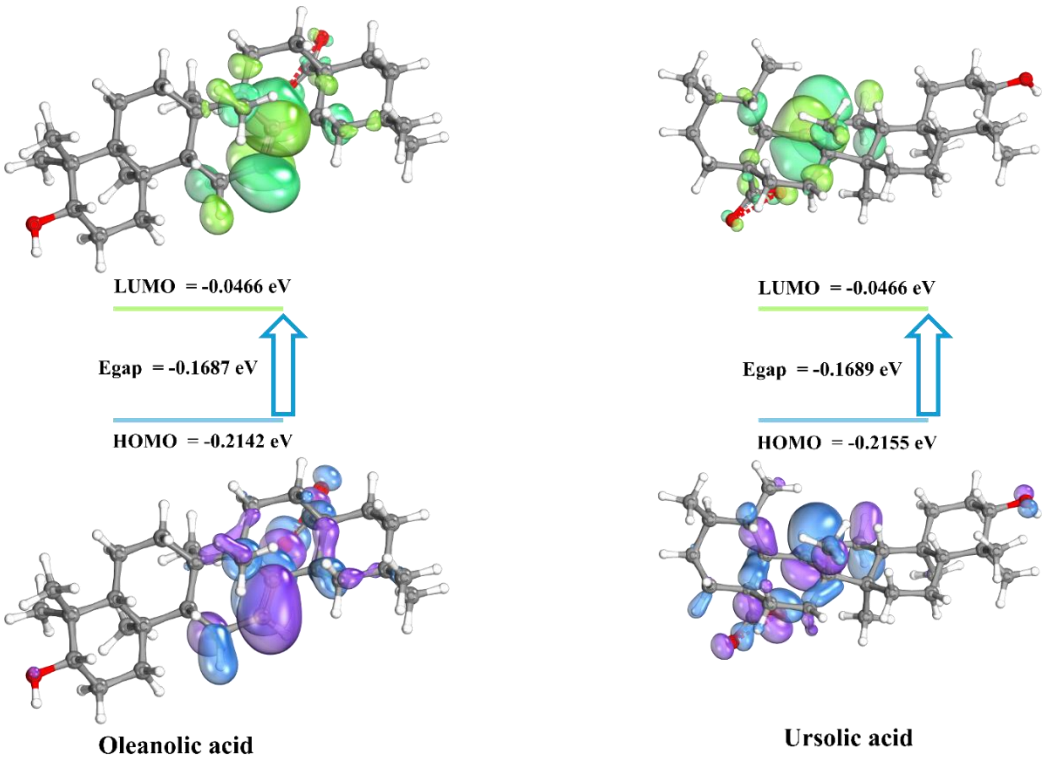

Figure 7. 3D visualization of HOMO and LUMO charge density. Visualization was done using IboView.

This study conducted a molecular electrostatic potential (MEP) visualization using the Avogadro software. The MEP maps of oleanolic acid and ursolic acid, selected as lead inhibitor candidates based on binding energy evaluation, molecular interaction analysis, and ADME-PASS profiling, are presented in Figures 8 and 9, respectively. These MEP visualizations aid in understanding the distribution of electrostatic potential and offer insight into reactive sites relevant to chemical reactions involving electrophilic and nucleophilic interactions. The MEP maps for oleanolic acid and ursolic acid provide a comprehensive depiction of each molecule's size, shape, and charge distribution. In the 3D representations, red regions indicate areas of negative electrostatic potential, white denotes neutral potential, and increasingly blue regions reflect areas of positive potential, corresponding to the color gradient used in Figures 8 and 9. The red zones indicate regions favorable for electrophilic attack, whereas the blue regions indicate regions susceptible to nucleophilic interactions. Previous pharmacological studies have employed MEP analysis to identify potential sites of biological inhibition, thereby supporting rational drug design [31–34].

The MEP analysis facilitated the identification of electrophilic and nucleophilic sites within the molecular system in a biological context, thereby providing insight into reactive biological activity. In this study, distinct polar and nonpolar regions of the selected molecules were identified, and these regions were visually represented using a range of color gradients. As shown in Figures 8 and 9, a prominent positive region appears around the hydrogen (H) atoms, indicating potential sites with positive charge (blue and light blue). Based on the MEP plot, the oxygen atoms within the hydroxyl groups exhibit high electropositive potential (red), whereas moderately activated regions display slightly lower electropositive potential (blue). Regions susceptible to electrophilic attack correspond to the negatively charged areas observed in the MEP visualization [35].

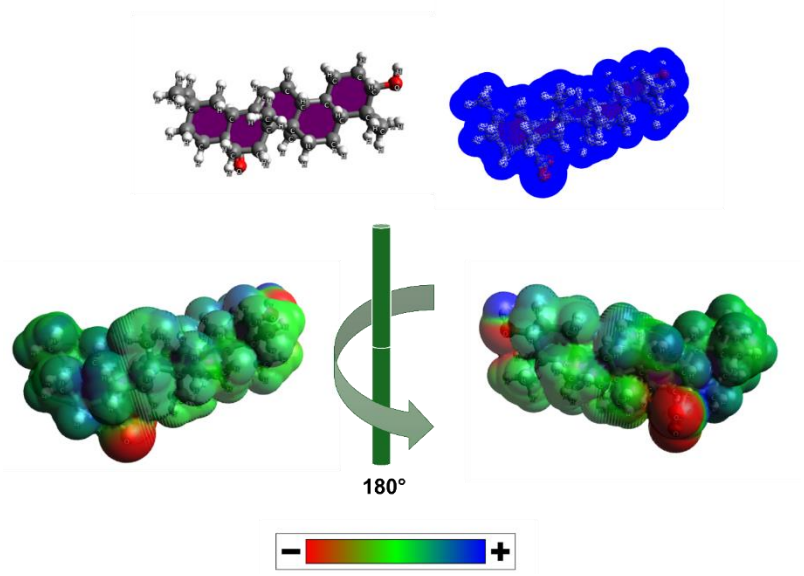

Figure 8. Molecular electrostatic potential (MEP) map of oleanolic acid.

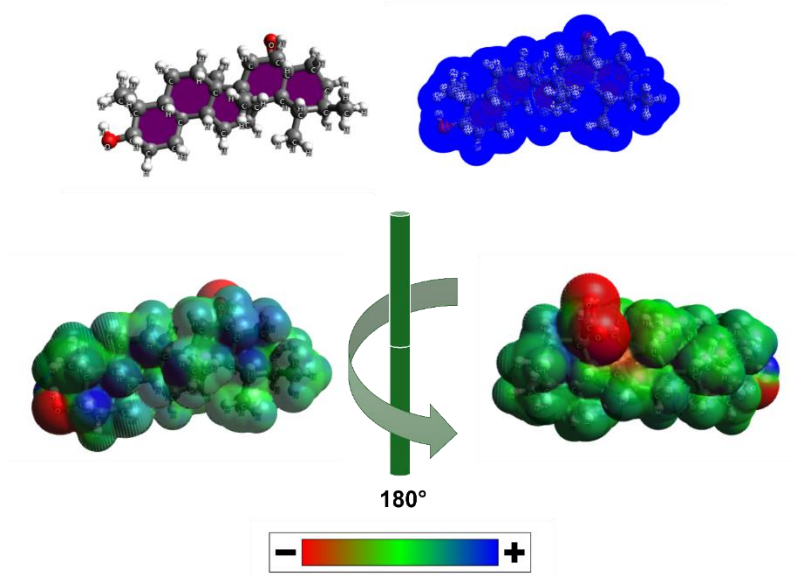

Figure 9. Molecular electrostatic potential (MEP) map of ursolic acid.

3.6. Post-dynamics analysis.

Normal mode analysis (NMA) was employed in this study to evaluate the physical motion and structural stability of protein–ligand complexes using the (.pdb) format. NMA has proven to be a valuable technique for uncovering essential functional insights by characterizing the accessible flexible states of a protein relative to its equilibrium position. It remains a widely used approach to study the dynamics of charged macromolecules [36]. The simulation results revealed that deformability analysis provides a means to assess atomic regions prone to structural deformation. In the context of proteins, hinge points, which are regions of high flexibility, can be inferred from zones exhibiting the greatest deformability. In other words, deformability enables interactive exploration of flexible regions, as illustrated in the CDPK3–oleanolic acid and CDPK4–ursolic acid complexes (Figures 10A and 11A), thereby helpingredict potential hinge locations along the protein backbone [37]. Furthermore, B-factor plots (Figures 10B and 11B) for the CDPK3–oleanolic acid and CDPK4–ursolic acid complexes offer insight into atomic mobility by identifying regions with differential motion and quantifying the extent of atomic displacement from their equilibrium positions. Taken

together, deformability and mobility represent two complementary parameters that, although distinct in nature, collectively enhance our understanding of protein flexibility and dynamics [37].

Figures 10C and 11C present the eigenvalue parameters, which represent the vibrational modes within the CDPK3–oleanolic acid and CDPK4-ursolic acid complexes. These vibrational modes, derived from NMA, are instrumental in identifying low-frequency motions that are often crucial for biological function [38]. Further details regarding variance are illustrated by purple bars, while cumulative variance is shown in green for each respective complex (Figures 10D and 11D). It is important to note that the variance was inversely proportional to the eigenvalue, providing a quantitative assessment of motion flexibility (Figures 10D and 11D). The elastic network models displayed in Figures 10E and 11E depict the connectivity and constraint relationships between residues within the CDPK3–oleanolic acid and CDPK4–ursolic acid complexes, respectively [39]. Meanwhile, the covariance matrix (Figures 10F and 11F) provides insight into residue motion correlations: correlated movements are indicated in red, anticorrelated movements in blue, and uncorrelated regions in white. Collectively, these comprehensive NMA evaluations offer valuable insights into the mechanisms of ligand-protein interaction further supporting the assessment of potential therapeutic efficacy [15,38]. In addition, the overall NMA profiles demonstrated minimal large-scale fluctuations and relatively high eigenvalues, suggesting that both CDPK3–oleanolic acid and CDPK4–ursolic acid complexes maintain stable conformations with restricted flexibility. The limited deformation and consistent energy distribution observed throughout the simulations reflect stable ligand binding within the active site, analogous to the interpretation of low RMSD and steady energy fluctuation in classical MD analysis.

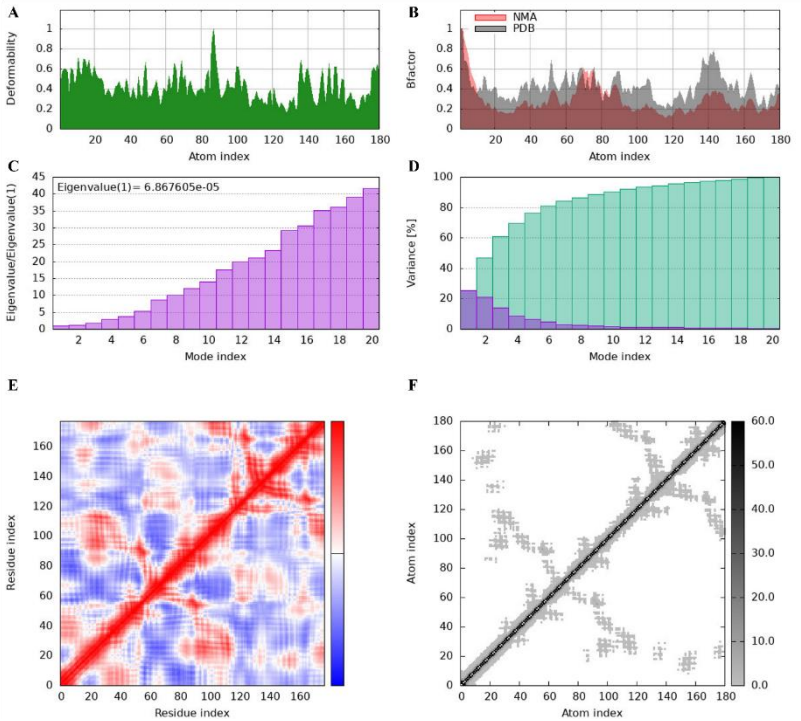

Figure 10. Molecular dynamics evaluation of the CDPK3-oleanolic acid complex, **(A)** Deformability graphs; **(B)** B-factor plots; **(C)** eigenvalue plots; (**D**) variance map plots; **(E)** Correlation matrix plots; **(F)** elastic network of complex.

This stability further supports the reliability of these complexes as potential inhibitors. To the best of our knowledge, the NMA approach used to investigate the CDPK3–ligand and CDPK4–ligand complexes represents a novel application introduced for the first time in this

study. Therefore, this investigation is expected to provide broader insights into the inhibition mechanisms of both target receptors. Nkungli *et al*. [40] presented an *in silico* investigation of falcipain-2 inhibition by hybrid benzimidazole–thiosemicarbazone antiplasmodial compounds, and in their molecular dynamics simulations, the study employed the GROMACS 2022 software package. Similarly, a study by Dhingra et al. [41] reported the use of MD simulations with GROMACS 2021.3 to evaluate the stability of receptor–ligand complexes, specifically targeting Plasmodium falciparum dihydroorotate dehydrogenase.

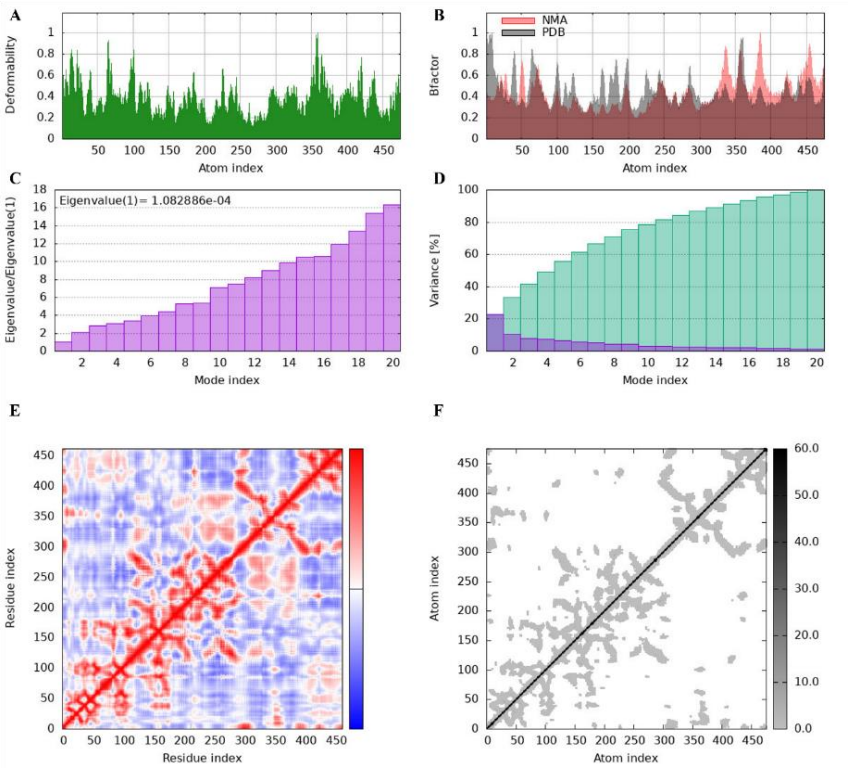

Figure 11. Molecular dynamics evaluation of the CDPK4-ursolic acid complex, **(A)** Deformability graphs; **(B)** B-factor plots; **(C)** eigenvalue plots; **(D)** variance map plots; **(E)** Correlation matrix plots; **(F)** elastic network of complex.

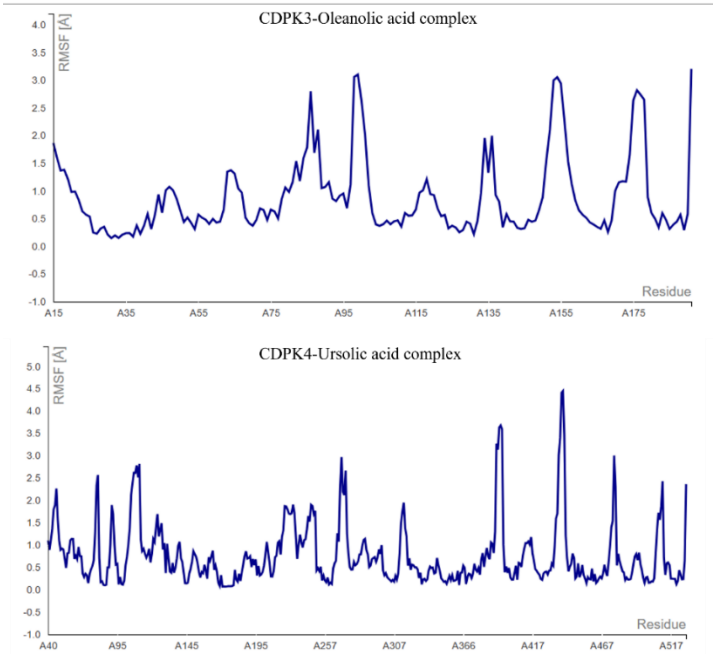

Figure 12. RMSF graph. The graph was generated using CABS-flex.

To further assess the stability of the CDPK3-4 complexes with potential inhibitors, the Root Mean Square Fluctuation (RMSF) profiles from MD simulations were examined. RMSF analysis, conducted using CABS-flex, explicitly revealed the flexibility of each amino acid residue, as illustrated in Figure 12. According to the results shown in Figure 12, higher RMSF values indicate greater flexibility, whereas lower values reflect restricted atomic motion within the system throughout the simulation period [42].

This study employed a fully *in silico*–based computational approach. The absence of laboratory-based validation represents a key limitation of the present research. Computer-aided drug design (CADD) has rapidly evolved and is now integrated into modern drug discovery pipelines. However, despite its advancement, CADD still faces several critical challenges and gaps, particularly in optimizing methodological efficiency, reliability, and applicability. One of the major constraints in CADD remains the availability and quality of both biological and chemical datasets. Additionally, the lack of standardization in integrating large-scale biological data, such as genomics, proteomics, and metabolomics (multi-omics), poses significant hurdles for CADD-based studies. The incorporation of artificial intelligence (AI) and machine learning (ML) into CADD has transformed the field. Yet, many predictive models suffer from overfitting, limited interpretability, and poor generalizability across diverse chemical spaces [43]. Despite these limitations, this study leveraged high-performance computing (HPC), which, while powerful, often involves high operational costs and limited accessibility. Nevertheless, the current research addresses emerging challenges and proposes a novel perspective for exploring potential antimalarial drug candidates. For future studies and to validate the findings of this research, laboratory-based experiments will be required, including *in vitro* assays, *in vivo* testing using animal models, and even mutant animal models. These approaches are essential for confirming the consistency between in silico computational predictions and in vitro experimental outcomes.

4. Conclusions

This study presents a comprehensive *in silico* analysis of CDPK3 and CDPK4 from *Plasmodium falciparum* in response to the growing challenge of malaria drug resistance. Among the screened compounds from *Hippophae rhamnoides* L. (Sea buckthorn), oleanolic acid and ursolic acid were identified as the most promising inhibitors, exhibiting strong binding affinities, stable molecular interactions, and comparable electronic reactivity, as determined by DFT calculations. The findings further validate CDPK3 and CDPK4 as druggable protein targets, supporting a dual-target inhibition strategy that may simultaneously disrupt parasite development and transmission. Nevertheless, *in vitro* and *in vivo* studies remain essential to confirm the biological efficacy and pharmacological safety of these compounds.

While computational predictions provide a robust preliminary foundation, they inherently lack the biological complexity of living systems, such as metabolic transformations, cellular uptake, off-target effects, and immune responses. Therefore, bridging this translational gap requires systematic laboratory validation. Experimental studies remain essential to confirm the biological efficacy, toxicity, and pharmacological properties of the proposed inhibitors. Finally, this study not only reinforces CDPK3 and CDPK4 as viable and druggable therapeutic targets but also highlights the phytochemical potential of sea buckthorn as a valuable source for next-generation antimalarial agents.

Author Contributions

Conceptualization, W.N., G.M.G., and M.A.D.; methodology, W.N., G.M.G., R.A.P.I., M.A.D., and F.R.M.; software, W.N. and G.M.G.; validation, W.N., G.M.G., R.A.P.I., M.A.D., F.R.M., E.S.S., F.S., D.H., and R.M.A.; formal analysis, W.N., G.M.G., R.A.P.I., M.A.D., F.R.M., E.S.S., F.S., D.H., and R.M.A.; investigation, W.N. and G.M.G.; resources, W.N. and G.M.G.; data curation, W.N., G.M.G., R.A.P.I., M.A.D., F.R.M., E.S.S., F.S., D.H., and R.M.A.; writing—original draft preparation, W.N. and G.M.G.; writing—review and editing, W.N., G.M.G., R.A.P.I., M.A.D., F.R.M., E.S.S., F.S., D.H., and R.M.A.; visualization, G.M.G.; supervision, W.N. All authors have read and agreed to the published version of the manuscript.

Institutional Review Board Statement

Not applicable.

Informed Consent Statement

Not applicable.

Data Availability Statement

Data supporting the findings of this study are available upon reasonable request from the corresponding author.

Funding

This research received no external funding.

Acknowledgments

None.

Conflicts of Interest

The authors declare no conflict of interest.

References

1. Gordzevich, R.; Brown, E.D. Host-like conditions validate nutrient transport as an antimalarial drug target. *Cell Chem. Biol.* **2025**, *32*, 777–779, https://doi.org/10.1016/j.chembiol.2025.05.006.
2. Dash, M.; Sachdeva, S.; Bansal, A.; Sinha, A. Gametogenesis in *Plasmodium*: Delving Deeper to Connect the Dots. *Front. Cell. Infect. Microbiol.* **2022**, *12*, 877907, https://doi.org/10.3389/fcimb.2022.877907.
3. Bansal, A.; Molina-Cruz, A.; Brzostowski, J.; Mu, J.; Miller Louis, H. *Plasmodium falciparum* Calcium-Dependent Protein Kinase 2 Is Critical for Male Gametocyte Exflagellation but Not Essential for Asexual Proliferation. *mBio* **2017**, *8*, 10-1128, https://doi.org/10.1128/mBio.01656-17.
4. Ghartey-Kwansah, G.; Yin, Q.; Li, Z.; Gumpper, K.; Sun, Y.; Yang, R.; Wang, D.; Jones, O.; Zhou, X.; Wang, L.; Bryant, J.; Ma, J.; Boampong, J.N.; Xu, X. Calcium-dependent Protein Kinases in Malaria Parasite Development and Infection. *Cell Transplantation* **2020**, *29*, 0963689719884888, https://doi.org/10.1177/0963689719884888.
5. Mihal, M.; Roychoudhury, S.; Sirotkin, A.V.; Kolesarova, A. Sea buckthorn, its bioactive constituents, and mechanism of action: potential application in female reproduction. *Front. Endocrinol.* **2023**, *14*, 1244300, https://doi.org/10.3389/fendo.2023.1244300.

6. Żuchowski, J. Phytochemistry and pharmacology of sea buckthorn (*Elaeagnus rhamnoides*; syn. *Hippophae rhamnoides*): progress from 2010 to 2021. *Phytochem. Rev.* **2023**, *22*, 3–33, https://doi.org/10.1007/s11101-022-09832-1.
7. Kato, K.; Sudo, A.; Kobayashi, K.; Sugi, T.; Tohya, Y.; Akashi, H. Characterization of *Plasmodium falciparum* calcium-dependent protein kinase 4. *Parasitol. Int.* **2009**, *58*, 394-400, https://doi.org/10.1016/j.parint.2009.08.001.
8. Wernimont, A.K.; Amani, M.; Qiu, W.; Pizarro, J.C.; Artz, J.D.; Lin, Y.-H.; Lew, J.; Hutchinson, A.; Hui, R. Structures of parasitic CDPK domains point to a common mechanism of activation. *Protein Struct. Funct. Bioinform.* **2011**, *79*, 803-820, https://doi.org/10.1002/prot.22919.
9. Mahdeen, A.A.; Arpa, S.H.; Hasan, M.R.; Barua, L.; Ferdous, J.; Masum, M.H.U. Next-gen vaccine design: Integrating proteomics and bioinformatics for japanese encephalitis. *Comput. Struct. Biotechnol. Rep.* **2025**, *2*, 100049, https://doi.org/10.1016/j.csbr.2025.100049.
10. Pundir, S.; Garg, P.; Dviwedi, A.; Ali, A.; Kapoor, V.K.; Kapoor, D.; Kulshrestha, S.; Lal, U.R.; Negi, P. Ethnomedicinal uses, phytochemistry and dermatological effects of *Hippophae rhamnoides* L.: A review. *J. Ethnopharmacol.* **2021**, *266*, 113434, https://doi.org/10.1016/j.jep.2020.113434.
11. Land, H.; Humble, M.S. YASARA: A Tool to Obtain Structural Guidance in Biocatalytic Investigations. In Protein Engineering: Methods and Protocols; Bornscheuer, U.T., Höhne, M., Eds.; Springer New York: New York, NY, **2018**; pp. 43-67, https://doi.org/10.1007/978-1-4939-7366-8_4.
12. Yin, J.; Waman, V.P.; Sen, N.; Firdaus-Raih, M.; Lam, S.D.; Orengo, C. Understanding the structural and functional diversity of ATP-PPases using protein domains and functional families in the CATH database. *Structure* **2025**, *33*, 613-631.e616, https://doi.org/10.1016/j.str.2024.12.016.
13. Xu, Y.; Wang, S.; Hu, Q.; Gao, S.; Ma, X.; Zhang, W.; Shen, Y.; Chen, F.; Lai, L.; Pei, J. CavityPlus: a web server for protein cavity detection with pharmacophore modelling, allosteric site identification and covalent ligand binding ability prediction. *Nucleic Acids Res.* **2018**, *46*, W374-W379, https://doi.org/10.1093/nar/gky380.
14. Murugesan, R.; Kaleeswaran, B. *In silico* drug discovery: Unveiling potential targets in *Plasmodium falciparum*. *Asp. Mol. Med.* **2024**, *3*, 100038, https://doi.org/10.1016/j.amolm.2024.100038.
15. Alsedfy, M.Y.; Ebnalwaled, A.A.; Moustafa, M.; Said, A.H. Investigating the binding affinity, molecular dynamics, and ADMET properties of curcumin-IONPs as a mucoadhesive bioavailable oral treatment for iron deficiency anemia. *Sci. Rep.* **2024**, *14*, 22027, https://doi.org/10.1038/s41598-024-72577-8.
16. Kaur, G.; Das, N. Molecular cloning, expression and *in silico* analyses of calcium-dependent protein kinase 2 (CDPK2) in potato (*Solanum tuberosum* L.). *S. Afr. J. Bot.* **2022**, *148*, 634–642, https://doi.org/10.1016/j.sajb.2022.04.018.
17. Taghipour, A.; Tavakoli, S.; Sabaghan, M.; Foroutan, M.; Majidiani, H.; Soltani, S.; Badri, M.; Ghaffari, A.D.; Soltani, S. Immunoinformatic Analysis of Calcium-Dependent Protein Kinase 7 (CDPK7) Showed Potential Targets for *Toxoplasma gondii* Vaccine. *J. Parasitol. Res.* **2021**, *2021*, 9974509, https://doi.org/10.1155/2021/9974509.
18. Adelusi, T.I.; Ojo, T.O.; Bolaji, O.Q.; Oyewole, M.P.; Olaoba, O.T.; Oladipo, E.K. Predicting *Plasmodium falciparum* kinase inhibitors from antimalarial medicinal herbs using computational modeling approach. *In Silico Pharmacol.* **2023**, *12*, 4, https://doi.org/10.1007/s40203-023-00175-z.
19. Choudhuri, S.; Ghosh, B. Computational approach for decoding malaria drug targets from single-cell transcriptomics and finding potential drug molecule. *Sci. Rep.* **2024**, *14*, 24064, https://doi.org/10.1038/s41598-024-72427-7.
20. Abubakari, I.; Kwiyukwa, L.P.; Paul, L. Computational analysis of luteolin, apigenin and their derivatives from *Allophylus africanus* as potential inhibitors of plasmepsin II a malaria target. *BMC Chem.* **2025**, *19*, 196, https://doi.org/10.1186/s13065-025-01527-w.
21. Sheik Amamuddy, O.; Veldman, W.; Manyumwa, C.; Khairallah, A.; Agajanian, S.; Oluyemi, O.; Verkhivker, G.M.; Tastan Bishop, Ö. Integrated Computational Approaches and Tools for Allosteric Drug Discovery. *Int. J. Mol. Sci.* **2020**, *21*, 847, https://doi.org/10.3390/ijms21030847.
22. Lobato-Tapia, C.A.; Moreno-Hernández, Y.; Olivo-Vidal, Z.E. In Silico Studies of Four Compounds of *Cecropia obtusifolia* against Malaria Parasite. *Molecules* **2023**, *28*, 6912, https://doi.org/10.3390/molecules28196912.
23. Hafiz, A.; Bakri, R.; Alsaad, M.; Fetni, O.M.; Alsubaihi, L.I.; Shamshad, H. In Silico Prediction of *Plasmodium falciparum* Cytoadherence Inhibitors That Disrupt Interaction between gC1qR-DBLβ12 Complex. *Pharmaceuticals* **2022**, *15*, 691, https://doi.org/10.3390/ph15060691.

24. Mahamba, L.; Isa, M.A.; Kappo, A.P. *In silico* identification of potential inhibitors for the universal stress G4LZI3 protein from *Schistosoma mansoni* using molecular docking and molecular dynamics simulation analyses. *Asp. Mol. Med.* **2025**, *5*, 100084, https://doi.org/10.1016/j.amolm.2025.100084.
25. Giraudo, A.; Bolchi, C.; Pallavicini, M.; Di Santo, R.; Costi, R.; Saccoliti, F. Uncovering the Mechanism of Action of Antiprotozoal Agents: A Survey on Photoaffinity Labeling Strategy. *Pharmaceuticals* **2025**, *18*, 28, https://doi.org/10.3390/ph18010028.
26. Kleandrova, V.V.; Cordeiro, M.N.D.S.; Speck-Planche, A. In Silico Approach for Early Antimalarial Drug Discovery: De Novo Design of Virtual Multi-Strain Antiplasmodial Inhibitors. *Microorganisms* **2025**, *13*, 1620, https://doi.org/10.3390/microorganisms13071620.
27. Masnabadi, N.; Thalji, M.R.; Alhasan, H.S.; Mahmoodi, Z.; Soldatov, A.V.; Ali, G.A.M. Structural, Electronic, Reactivity, and Conformational Features of 2,5,5-Trimethyl-1,3,2-diheterophosphinane-2-sulfide, and Its Derivatives: DFT, MEP, and NBO Calculations. *Molecules* **2022**, *27*, 4011, https://doi.org/10.3390/molecules27134011.
28. Kunduracioglu, A. A Computational (DFT) Study on the Anti-Malarial Drug: Lumefantrine. *Appl. Sci.* **2023**, *13*, 9219, https://doi.org/10.3390/app13169219.
29. Abisek, A.; Poovarasan, R.; Sathish, T.; Tamizharasan, G.; Khute, S.; Rao, K.S.; Rajesh, A.; Subash, P. LC-MS/HRMS-guided identification and *In Silico* evaluation of *Barleria buxifolia* root compounds targeting malarial PI4KIIIβ. *In Silico Res. Biomed.* **2025**, *1*, 100057, https://doi.org/10.1016/j.insi.2025.100057.
30. Alruwaili, M.; Alhassan, H.H.; Almutary, H.; Tahir ul Qamar, M. Computational identification of aspartic protease inhibitors for antimalarial drug development against *Plasmodium Vivax*. *Sci. Rep.* **2025**, *15*, 14824, https://doi.org/10.1038/s41598-025-98516-9.
31. Sultana, T.; Tasnim, J.; Talukder, M.W.H.; Mia, M.L.; Suchana, S.N.; Akter, F.; Saleh, M.A.; Afrin, M.F.; Uzzaman, M. Physicochemical and toxicological studies of some commonly used triazine-based herbicides; *In-silico* approach. *Informat. Med. Unlocked* **2023**, *42*, 101378, https://doi.org/10.1016/j.imu.2023.101378.
32. Afrin, M.F.; Kabir, E.; Noyon, M.R.O.K.; Bhuiyan, M.M.H.; Shimu, M.S.S.; Alam, M.J.; Uzzaman, M.; Talukder, M.W.H. Spectrochemical, medicinal, and toxicological studies of ketoprofen and its newly designed analogs; quantum chemical, and drug discovery approach. *Informat. Med. Unlocked* **2023**, *43*, 101399, https://doi.org/10.1016/j.imu.2023.101399.
33. Ali, A.; Khalid, M.; Abid, S.; Tahir, M.N.; Iqbal, J.; Ashfaq, M.; Kanwal, F.; Lu, C.; Rehman, M.F.u. Green Synthesis, SC-XRD, Non-Covalent Interactive Potential and Electronic Communication *via* DFT Exploration of Pyridine-Based Hydrazone. *Crystals* **2020**, *10*, 778, https://doi.org/10.3390/cryst10090778.
34. Alzain, A.A.; Elbadwi, F.A. Identification of novel TMPRSS2 inhibitors for COVID-19 using e-pharmacophore modelling, molecular docking, molecular dynamics and quantum mechanics studies. *Informat. Med. Unlocked* **2021**, *26*, 100758, https://doi.org/10.1016/j.imu.2021.100758.
35. Jayavel, P.; Ramasamy, V.; Amaladoss, N.; Renganathan, V.; Shupeniuk, V.I. A facile synthesis, characterization, DFT, ADMET and *in-silico* molecular docking analysis of novel 4-ethyl acridine-1,3,9 (2,4,10H)-trione. *Chem. Phys. Impact* **2024**, *8*, 100476, https://doi.org/10.1016/j.chphi.2024.100476.
36. Bauer, J.A.; Pavlović, J.; Bauerová-Hlinková, V. Normal Mode Analysis as a Routine Part of a Structural Investigation. *Molecules* **2019**, *24*, 3293, https://doi.org/10.3390/molecules24183293.
37. Garzón, J.I.; Kovacs, J.; Abagyan, R.; Chacón, P. DFprot: a webtool for predicting local chain deformability. *Bioinformatics* **2007**, *23*, 901-902, https://doi.org/10.1093/bioinformatics/btm014.
38. Maoz, H.; Elalouf, A.; Rosenfeld, A.Y. Bioinformatics-Based Management of Vitellogenin-like Protein's Role in Pathogen Defense in *Nicotiana tabacum* L. *Appl. Sci.* **2025**, *15*, 4463, https://doi.org/10.3390/app15084463.
39. Chundru, D.; Bhattrai, S.; Timilsina, M.; Lillehoj, H.; Sun, Z.; Ghanem, M.; Li, C. In Silico Design, Optimization, and Evaluation of a Multi-Epitope Vaccine Targeting the *Clostridium perfringens* Collagen Adhesin Protein. *Microorganisms* **2025**, *13*, 1147, https://doi.org/10.3390/microorganisms13051147.
40. Nkungli, N.K.; Fouegue, A.D.T.; Tasheh, S.N.; Bine, F.K.; Hassan, A.U.; Ghogomu, J.N. In silico investigation of falcipain-2 inhibition by hybrid benzimidazole-thiosemicarbazone antiplasmodial agents: A molecular docking, molecular dynamics simulation, and kinetics study. *Mol. Divers.* **2024**, *28*, 475-496, https://doi.org/10.1007/s11030-022-10594-3.
41. Dhingra, N.; Mourya, A.; Singh, H.; Prajapati, N. Exploring QSAR, molecular docking, molecular dynamics and pharmacokinetics for 3,4-Dihydro-2H,6H-pyrimido[1,2-c][1,3]benzothiazin-6-imine derivatives targeting *Plasmodium falciparum* dihydroorotate dehydrogenase. *Discov Chem.* **2025**, *2*, 104, https://doi.org/10.1007/s44371-025-00170-7.

42. Sumera; Anwer, F.; Waseem, M.; Fatima, A.; Malik, N.; Ali, A.; Zahid, S. Molecular Docking and Molecular Dynamics Studies Reveal Secretory Proteins as Novel Targets of Temozolomide in Glioblastoma Multiforme. *Molecules* **2022**, *27*, 7198, https://doi.org/10.3390/molecules27217198.
43. Mihai, D.P.; Nitulescu, G.M. Computer-Aided Drug Design and Drug Discovery. *Pharmaceuticals* **2025**, *18*, 436, https://doi.org/10.3390/ph18030436.

Publisher's Note & Disclaimer